

OPEN Soft and wrinkled carbon membranes derived from petals for flexible supercapacitors

Received: 06 December 2016 Accepted: 23 February 2017 Published: 31 March 2017 Xiuxiu Yu^{1,*}, Ying Wang^{1,*}, Li Li^{2,3}, Hongbian Li^{2,3} & Yuanyuan Shang¹

Biomass materials are promising precursors for the production of carbonaceous materials due to their abundance, low cost and renewability. Here, a freestanding wrinkled carbon membrane (WCM) electrode material for flexible supercapacitors (SCs) was obtained from flower petal. The carbon membrane was fabricated by a simple thermal pyrolysis process and further activated by heating the sample in air. As a binder and current collector-free electrode, the activated wrinkled carbon membrane (AWCM) exhibited a high specific capacitance of 332.7 F/g and excellent cycling performance with 92.3% capacitance retention over 10000 cycles. Moreover, a flexible all-solid supercapacitor with AWCM electrode was fabricated and showed a maximum specific capacitance of 154 F/q and great bending stability. The development of this flower petal based carbon membrane provides a promising costeffective and environmental benign electrode material for flexible energy storage.

To meet the ever-growing demand of clean energy, energy storage is highly desirable. Supercapacitors (SCs) with high power density, fast charging rate and excellent cycling performance, have attracted great attention as a high-efficient energy storage device¹⁻³. In SCs, electrical double layer capacitor (EDLC) is one of the main type, which mainly bases on the accumulation of ions at the interface between electrode and electrolyte4. For the electrode materials of EDLC, porous carbon has been considered as an ideal candidate due to its high specific surface area (SSA), good conductivity and electrochemical stability. Particularly, in recent few years, nanocarbons like carbon nanotubes and graphene have been extensively explored as the electrode materials for EDLCs with excellent electrochemical performance⁵⁻⁹. However, the synthesis of these nanocarbons suffers from the drawbacks of the high cost chemical vapor deposition (CVD) process or the environmental issues related to the usage of toxic chemicals. Therefore, development of green methods to fabricate low-cost and high performance carbon materials in large scale is critical for the practical application of EDLCs.

Biomass derived carbon provides a promising electrode material with a low cost and environmental friendly fabrication process¹⁰. A range of biomasses, such as leaves¹¹, pomelo peels¹², willow catkins^{13,14}, chicken egg-shell membranes¹⁵, seaweeds¹⁶, elm samara¹⁷, silk^{18,19}, sugar cane bagasses²⁰ and coffee beans²¹ have been used as the precursor to fabricate porous carbon with high specific capacitance and cycling stability. However, polymer binders are always used to be mixed with these porous carbon materials to form the electrodes, which requires extra steps and also obstructs pores, resulting a reduced specific capacitance²². To avoid the extra mixing process and simplify the device fabrication process, a freestanding, binder and current collector-free carbon electrode is

Recently, freestanding carbon electrodes have been fabricated from carbonization of bacterial cellulose²³, watermelon²⁴ and cotton²⁵. However, these carbon electrodes are in the form of a three-dimensional porousblock, showing limited flexibility in the as-prepared devices. Flower petals, as one of the most abundant biomass sources, can be carbonized into a freestanding carbon membrane by a simple one-step thermal pyrolysis process. Unlike other flat nature materials, the thickness of the flower petals is only 10-20 μm, resulting in a high flexibility of the carbonized petal membranes. Another advantage of these carbon membranes is that they inherit the wrinkled surface of the flower petals, which show high SSA for ions storage. Therefore, flower petal based carbon membranes are very promising as the electrodes for flexible SCs.

¹School of Physical Engineering, Zhengzhou University, Zhengzhou, Henan, 450052, China. ²CAS Center for Excellence in Nanoscience, National Center for Nanoscience and Technology, Beijing, 100190, China. 3 University of Chinese Academy of Sciences, Beijing, 100049, China. *These authors contributed equally to this work. Correspondence and requests for materials should be addressed to H.L. (email: lihb@nanoctr.cn) or Y.S. (email: yuanyuanshang@zzu.edu.cn)

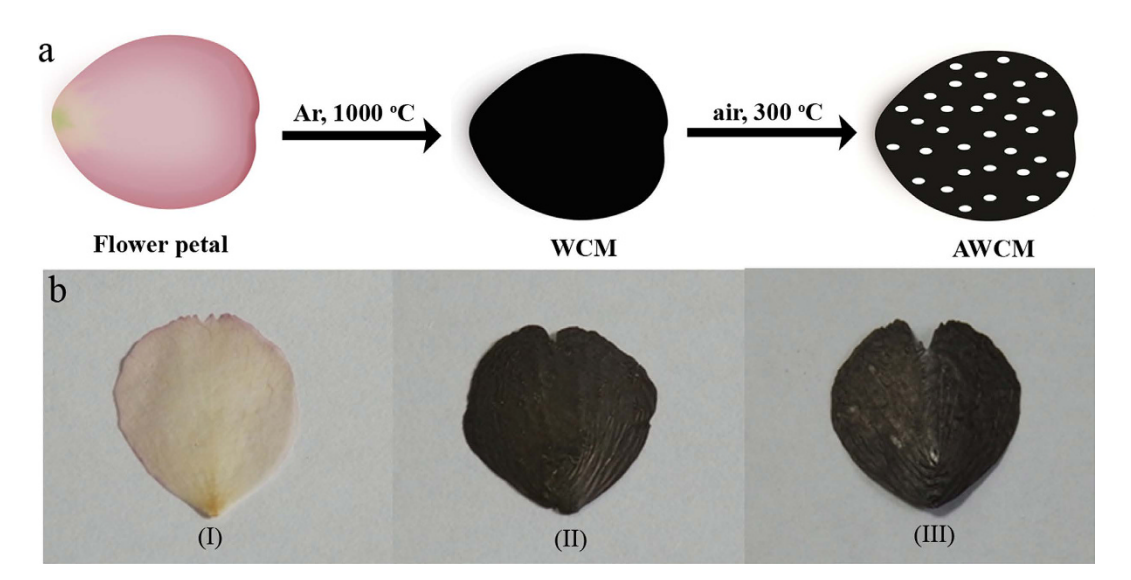


Figure 1. (a) Schematic illustration of the fabrication process of the WCM and AWCM, where a carbonization and activation two-step method was adopted. (b) The images of a petal at different stages: (I) dry petal, (II) carbonized petal and (III) activated carbonized petal.

In the present work, flexible and wrinkled carbon membrane (WCMs) were membranes prepared by carbonizing flower petals for the first time. After an activation process by heating the WCMs in air, AWCMs with a high specific surface area $(509\,\mathrm{m^2/g})$ were obtained. Unlike carbonaceous materials derived from other reported biomasses, no additional binder and current collector are needed, which greatly simplified the device fabrication process of the supercapacitors. The AWCM exhibits a maximum specific capacitance of $332.7\,\mathrm{F/g}$ at $10\,\mathrm{mV/s}$ and excellent cycling performance. Furthermore, the carbon membrane is highly flexible and a symmetric all-solid SC with high flexibility was fabricated, which exihibits a specific capacity of $154\,\mathrm{F/g}$, outperforming other porous carbon based SCs. The performance of the device under bending is very stable and no apparent capacitance decay was found after 10 bending cycles.

Results and Discussion

Synthesis and morphologies of wrinkled carbon membranes. The flower petals used in this paper are those from Cherry blossom collected in the campus of Zhengzhou University. Preparation of WCM and ACWM is briefly illustrated in Fig. 1a and the detailed experimental description is provided in the methods part. WCM was prepared by a thermal pyrolysis process at 1000 °C under the protection of Ar. After the carbonization process, the color of the petal changed from light pink to black, indicating the successful transformation of the petal into carbon membrane. To increase the SSA of the WCM, the as prepared carbon membrane was further heated at 300 °C in air. The activation mechanism is mainly based on the removal of active carbon atoms at the defects, which is similar as the pore fabrication process in graphene⁹. As shown in Fig. 1b, both WCM and AWCM maintained well the original structure of the petal, indicating a good mechanical strength as a freestanding membrane for EDLCs. Compared with those carbon materials activated by KOH and ZnCl₂ that only carbon powder can be obtained ^{15,20}, mildly thermal treatment of the petals in air is beneficial to maintain their unique structure.

To reveal the structure of the carbonized membrane, scanning electron microscopy (SEM) and transmission electron microscopy (TEM) of the AWCM were performed. As shown in Fig. 2a,b and Figure S1, both AWCM and WCM inherited the hierarchy structure of the original petals. As indicated with yellow lines in Fig. 2b, the surface is made up of many wrinkled quadrangle, pentagonal and hexagonal domains of about 10 µm in width and 20 µm in length. From the magnified SEM image of a single domain in Fig. 2c, a lot of subwrinkles can be clearly observed. The height of the wrinkle is around 5-10 nm and the distance between each wrinkle is around 3-5 µm. The inner structure of the AWCM is displayed by the SEM image for the cross-section part from Fig. 2d to Fig. 2f From Fig. 2d, each carbon membrane is made up of two pieces of wrinkled film stacking together with an inner gap of 1-3 µm between the films. The thickness of a single wrinkled film is only 700 nm, and the total thickness of the membrane is 5-10 µm. This small thickness guaranteed the flexibility of the carbon membrane to be flexible electrode for EDLCs. From the magnified image indicated by the circle in Fig. 2d, one can see there are also numerous smaller wrinkles in the inner side of the single membrane, as shown in Fig. 2f. This hierarchical porous structure endows the AWCM an excellent electrode to store ions in supercapacitors. TEM image in Fig. 2g and h provide further insight for the microstructure of the AWCM, where a thin film with short-range aligned crystal lattice indicates an amorphous carbon structure²⁶. Compared with the TEM image of the WCM (see Figure S2), more disordered carbon regions are observed, indicating that numerous pores are fabricated in the activation process, which reduced the ion-transport path and further increased the rate performance of the SCs²³.

Structures of wrinkled carbon membrane. Further structural information was investigated and the results are shown in Fig. 3. Figure 3a presents the X-ray diffraction (XRD) patterns of the WCM and AWCM. Two weak and broad peaks at 22.2° and 44° demonstrate the diffractions peaks of (200) and (100) planes of graphite¹⁸.

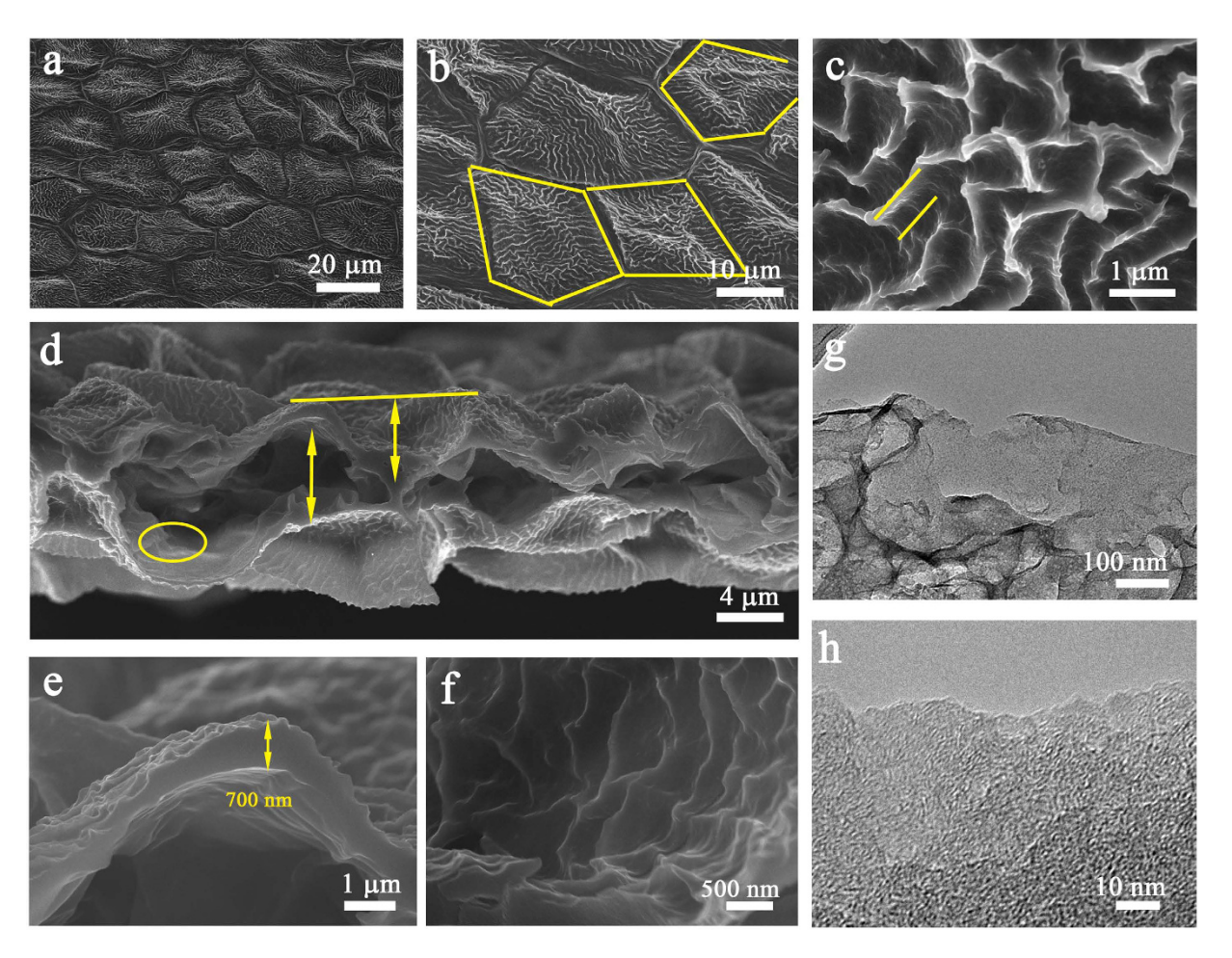


Figure 2. SEM and TEM images of AWCMs. (a) SEM and (b,c) magnified SEM images of the AWCM, showing the wrinkled surface. (d) SEM and (e,f) magnified SEM images of the cross-section of the AWCM. (g,h) TEM and magnified TEM images of the AWCM.

Compared with WCM, the diffraction peak at 22.2° of the AWCM is broadened, suggesting the lower graphitization degree of the AWCM²⁰, which is in accordance with the result of TEM. The Raman spectroscopy in Fig. 3b further confirms the lower degree of graphitization after activation. The two peaks corresponding to D band and G band locate at 1358 and 1589 cm⁻¹ for WCM and 1350 and 1609 cm⁻¹ for ACWM. The I_D/I_G increased from 0.79 to 0.88, indicating that the activation process has successfully increased the number of disordered carbon and lowered the graphitization degree²³. For SCs, SSA and pore structure are two critical factors that decide their specific capacitance and rate performance²⁷. In order to investigate the pore structure before and after activation, N₂ gas adsorption-desorption measurement was performed and the corresponding isotherms are provided in Fig. 3c. In comparison with WCM, the N₂ adsorption volume of AWCM increased greatly from 10 to 191.5 cubic centimeters (CCs) at one standard pressure, indicating a rapid increase in SSA. Calculated by the standard BET method, the SSA of the AWCM is 509 m²/g, which is 79 times higher than that of WCM (6.44 m²/g), confirming that simply heating in air can efficiently increase the SSA and maintain the mechanical strength of the petals at the same time. The pore size distribution in Fig. 3d shows that the intensity of peak for the pores at around 3.6 nm increased greatly for AWCM. The introduction of these pores facilitates the transport of the ions through the electrode materials and further increases their specific capacitances. In order to obtain the chemical composition of the WCM and AWCM, the samples were analyzed by X-ray photoelectron spectroscopy (XPS). As can be seen Figure S3, the content of the oxygen increased from 6.77% for WCM to 14.41% for AWCM by atoms. This increased oxygen content indicates that some carbon atoms are oxidized and many defects are created, which is in agreement with the result shown in Fig. 3b. The introduction of these oxygen containing functional groups is also beneficial to increase the specific capacitance²⁸.

Electrochemical evaluation of as-fabricated electrodes. The electrochemical performance of the WCM and AWCM as the electrode materials for EDLCs in a three-electrode system was evaluated in 0.5 M KCl electrolyte^{29–31}. Figure 4a is the cyclic voltammogram (CV) curve comparison of the WCM and AWCM electrode at the same scan rate of 50 mV/s, where the area enclosed by the quasi-rectangular CV curve of the AWCM is much larger than that of the WCM. The calculated specific capacitances of the AWCM and WCM are 253 and 105 F/g, respectively, resulting from the increased interface between the carbon membrane and the electrolyte and improved ion acceleration. Figure 4b exhibits the CV curves of the AWCM electrode at the scan rate from 10

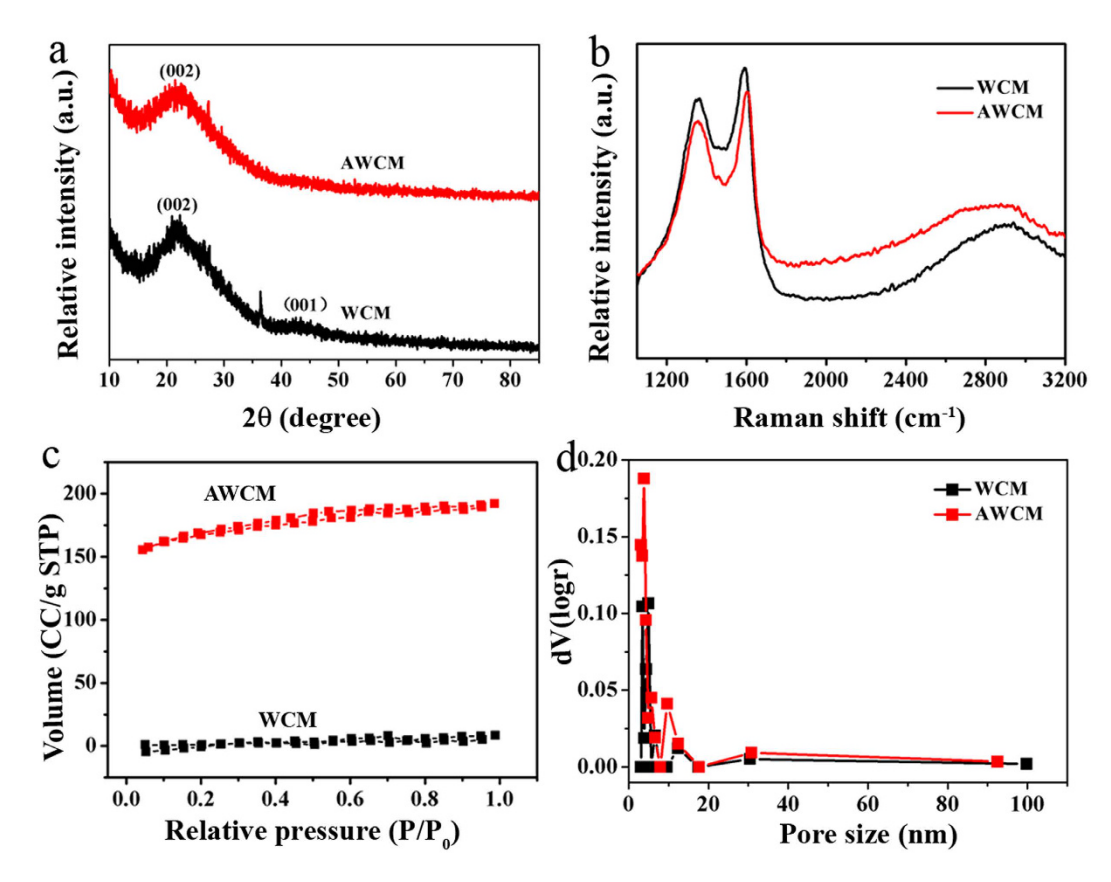


Figure 3. Structural analysis of the WCM and AWCM. (a) XRD patterns and (b) Raman spectrum comparison of the WCM and AWCM. (c,d) N_2 adsorption and desorption isotherm and pore size distribution of the WCM and AWCM.

to 200 mV/s. It can be seen that AWCM shows better rectangular shape than WCM (see Figure S4), which results from the higher porosity of the AWCM. The calculated specific capacitances of the WCM and AWCM at different scan rates are provided in Fig. 4c, with the maximum value of 146.8 and 332.7 F/g at 10 mV/s. It can be observed that the specific capacitance of both WCM and AWCM decrease with the increase of the scan rate, which is related to the limited ion diffusion on the electrode surfaces due to the fast charging. However, the performance of the AWCM is always better than that of WCM. The rate performance can be further improved by optimizing the activation process to tune the pore structure of the AWCM. The galvanostatic charge-discharge (GCD) curves of the AWCM at varied current densities from 10 to 50 A/g are displayed in Fig. 4d. The lines are almost symmetrical with slight distortion, indicating its good capacitive behavior. Electrochemical impedance spectroscopy (EIS) was carried out to study the charge transfer resistance within the WCM and AWCM based electrode. The Nyquist plot was collected over the frequency range from 0.01 Hz to 100 kHz at an open circuit voltage. As can be seen in Fig. 4e, for the AWCM, the line at the low frequency is almost vertical while that for WCM is a slope, demonstrating its better ion diffusion into the electrode structure. Furthermore, the appearance of the semicircle at the high frequency in the inset image also indicates a porous structure of the AWCM and better electrolyte intrusion in the electrode, which further facilitates a faster ion transport in the AWCM than that of WCM. To investigate the stability of the electrochemical performance of AWCM, the cyclic stability measurement was carried out. As shown in Fig. 4f, AWCM exhibits an excellent cycling performance. At a charge-discharge current density of 20 A/g over 10000 cycles, the capacitance retention is as high as 92.3%. This excellent stability is attributed to the stable ion adsorption-desorption process at the interface between AWCM and electrolyte.

The temperature of pyrolysis and activation plays an important role for the electrochemical performance of the carbon membrane electrode. Different carbon membranes were prepared under different pyrolysis temperatures at 600, 800, 1000 and 1200 °C separately, and the electrochemical performance comparison is shown in Figure S5. One can see the electrochemical performance of the electrode decreases under a lower or higher temperature, indicating 1000 °C is an appropriate temperature for the pyrolysis of the petals. Besides, we also studied the influence of the activation temperature on the electrochemical performance of the electrode. As shown in Figure S6, when the activation temperature increased from 300 to 400 °C, the specific capacitance dropped from 253.01 to 166.46 F/g. Therefore, the best activation temperature for the carbon membrane electrode is 300 °C.

To demonstrate the practical applications of AWCM, a flexible all-solid supercapacitor was fabricated, with AWCM as the electrode and $\rm H_3PO_4/Polyvinyl$ alcohol (PVA) gel as the solid electrolyte^{32–34}. The schematic illustration of the flexible supercapacitor is demonstrated in Fig. 5a. Figure 5b is a picture of the as-prepared device, which is highly flexible and can be bent into different angles. The CV curves of the device at different scan rates

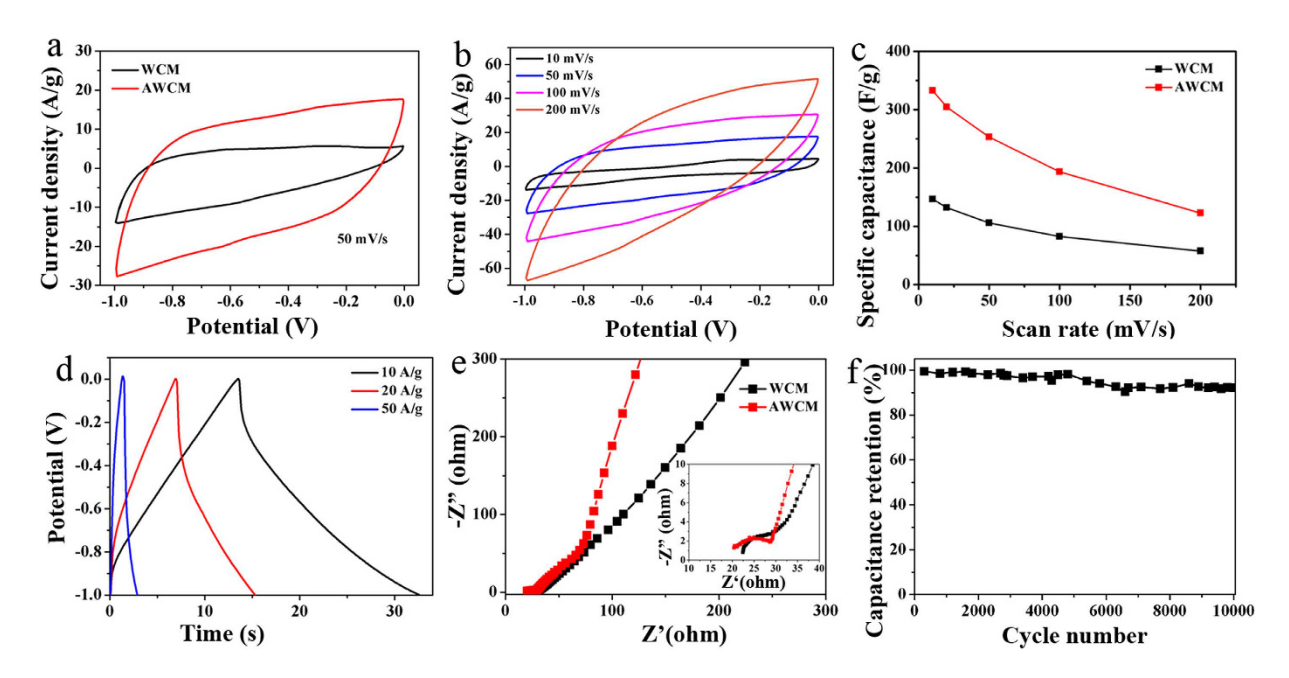


Figure 4. Electrochemical performance of the WCM and AWCM in EDLCs using aqueous electrolyte. (a) CV curves of the WCM and AWCM at a scan rate of 50 m V/s. (b) CV curves of the AWCM at different scan rates from 10 to 200 mV/s. (c) Specific capacitances calculated from CV curves as a function of scan rates. (d) GCD curves of AWCM at different discharge current densities. (e) Nyquist plots of the WCM and AWCM with the inset showing the high frequency region. (f) Capacitance retention of the AWCM over 10000 cycles.

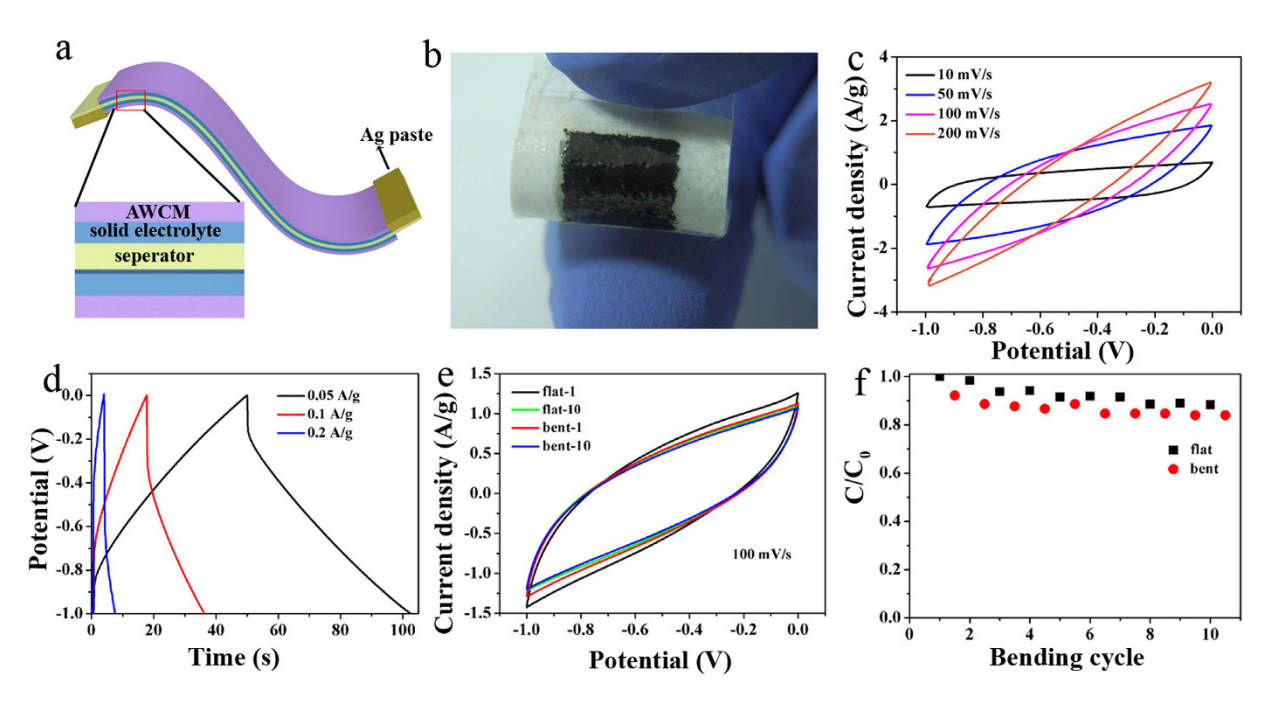


Figure 5. Electrochemical performance of the AWCM-based all-solid supercapacitor. (a) Schematic illustration of a flexible supercapacitor. (b) The image of the as-prepared supercapacitor. (c) CV curves of the device at different scan rates. (d) GCD curves of device obtained at different current densities. (e) CV curve comparison of the device at different bending times. (f) Capacitance retention of the device over 10 bending times.

from 10 to $200 \, \text{mV/s}$ are provided in Fig. 5c. A calculated specific capacitance of $154 \, \text{F/g}$ was obtained at a scan rate of $10 \, \text{mV/s}$, which is higher than other porous carbon based supercapacitors $^{12,35-37}$. Figure 5d presents the GCD curves of the device at different current densities from 0.05 to $0.2 \, \text{A/g}$, where the symmetrical triangles indicate the good capacitive performance of the electrode materials in the device. To reveal the influence of the flexibility on the electrochemical performance of the device, a mechanical bending test of the device was performed.

As can be seen in Fig. 5e, there is negligible change in the CV curves at a scan rate of $100\,\mathrm{mV/s}$ after 10 bending times, showing the stable electrochemical performance of the all-solid device towards the bending deformation. From the capacitance retention shown in Fig. 5f, it can be seen that the capacitance of the device after bending for 10 cycles is still more than 80% of the original one, which further confirms AWCM can work well as the electrode material for flexible EDLCs.

Conclusions

In summary, we have prepared a freestanding AWCM from abundant and renewable flower petals by a thermal pyrolysis and further activation process. The AWCM maintains the shape and mechanical strength of the original petals and inherites their wrinkled microstructure on the surfaces. With a thickness of only 5– $10\,\mu m$, the AWCM is flexible and can work as a binder and current collector-free electrode for SCs. With a three-electrode system in KCl electrolyte, the AWCM shows a specific capacitance of 332.7 F/g with an excellent cycling performance. The flexible all-solid supercapacitor with AWCM electrode shows a high specific capacitance of 154 F/g and good bending stability, where negligible capacitance decay was observed after 10 bending cycles. This provides a cost-effective and efficient electrode material for the energy storage for the flexible device.

Methods

Fabrication of WCM. Cherry blossom petals were collected on campus of Zhengzhou University and dried under a pressure between 200–500 Pa. The dried petals were put into a tube furnace and carbonized at 1000 °C for 1 h under Ar at a flow rate of 100 sccm. The temperature ramping rate of the furnace is 10 °C/min. To avoid curling, the petals were fastened between graphite slides during the carbonization process. After the reaction, the carbonized petals were immersed in 4.0 M HCl for 48 h to remove the inorganic impurities.

Fabrication of AWCM. The clean WCM was put into the tube furnace and heated at 300 °C in air for 1 h with a ramping rate of 10 °C/min. To make the sample fully exposed to the air, WCM was heated in a quartz boat directly without graphite slides clapping.

Materials morphology and structure characterization. The scanning electron microscopy (SEM) and transmission electron microscopy (TEM) were performed on Hitachi S-4800 and FEI Tecnai F20 instruments, respectively. X-ray diffraction (XRD) patterns were collected on PANalytical X'Pert Powder instrument with Cu Koirradiation. Raman spectras were collected using a Renishaw inVia Raman microscope with a laser wavelength of 514.5 nm. The N_2 gas adsorption was measured with a Micromeritics accelerated surface area porosimetry (NOVA 4200e, China) auto adsorption analyzer. The N_2 adsorption isotherms were obtained at 77 K, and the specific surface area (SSA) was obtained by Brunauer–Emmett–Teller (BET) analyses of the adsorption isotherms. X-ray photoelectron spectroscopy (XPS) measurement was carried out on an ESCALAB250Xi apparatus at base pressure of 1×10^{-9} mbar with and X-ray source of Al K α .

Preparation of the solid electrolyte. H_3PO_4 and polyvinyl alcohol (PVA) were used as the solid electrolyte in the supercapacitor. At first, $2 g H_3PO_4$ and 2 g PVA were put into 20 mL DI water in a round-bottom flask. Then the flask was put into a hot water bath of $90 \,^{\circ}$ C under stirring for several hours until H_3PO_4 and PVA were completely dissolved and a clear solution was obtained.

Fabrication of the supercapacitor. AWCM was first cut into rectangular strips of 6 mm*8 mm, then two strips of AWCMs were used as the electrodes for the supercapacitor. Ag wire was attached onto one side of each electrode to connect the AWCM to the external circuit, then gel PVA/ H_3PO_4 was coated onto both sides of the AWCM electrodes until the AWCM are totally immersed into PVA/ H_3PO_4 electrolyte. After that, the AWCM coated with PVA/ H_3PO_4 was placed in air at room temperature for 12h to evaporate the water in the electrolyte until a gel-like electrolyte was obtained. To separate the two electrodes, a piece of paper which is slightly larger than the electrode material was inserted between two pieces of AWCM. At last, the two pieces of electrodes were further fastened with insulate tape and a supercapacitor was obtained.

Electrochemical measurements. Electrochemical measurements were carried out at room temperature using electrochemical workstation (CorrTest CS2350). Cyclic voltammetry and galvanostatic charge-discharge tests were performed in a voltage window of -1-0 V at different scan rates and current densities, respectively. The electrochemical impedance spectroscopy measurements were performed at frequency range from 100 kHz to 0.01 Hz. The mechanical flexibility test was carried out by manual control.

When tested in a three-electrode system, for a single electrode, its specific capacitance, Cs (F/g), can be calculated from the CV curves by

$$C = (2sVm)^{-1} \int IdV \tag{1}$$

where s is the scan rate, V is the potential window, m is the mass of single electrode and I is current.

When asymmetric supercapacitor is charged, a voltage will build up across the two electrodes. The capacitance (C, F) of the device is calculated with the equation

$$C = (2sV)^{-1} \int IdV \tag{2}$$

For an ideal symmetric supercapacitor, the specific capacitance, Cs (F/g) for the active material can be derived from the capacitance of the device

$$Cs = 4C/m = 2(sVm)^{-1} \int IdV$$
(3)

where *m* is the total mass of the active material (AWCM).

References

- 1. Simon, P. & Gogotsi, Y. Materials for electrochemical capacitors. Nat. Mater. 7, 845-854 (2008).
- 2. Wang, Q., Yan, J. Z. & Fan, J. Carbon materials for high volumetric performance supercapacitors: design, progress, challenges and opportunities. *Energy Environ. Sci.* **9**, 729–762 (2016).
- 3. Qie, L. *et al.* Synthesis of functionalized 3D hierarchical porous carbon for high-performance supercapacitors. *Energy Environ. Sci.* **6,** 2497–2504 (2013).
- 4. Béguin, F., Presser, V., Balducci, A. & Frackowiak, E. Carbons and electrolytes for advanced supercapacitors. *Adv. Mater.* 26, 2219–2251 (2014).
- 5. Yu, J. L. et al. Omnidirectionally stretchable high-performance supercapacitor based on isotropic buckled carbon nanotube films. ACS Nano 10, 5204–5211 (2016).
- 6. Choi, C. S. et al. Flexible supercapacitor made of carbon nanotube yarn with internal pores. Adv. Mater. 26, 2059-2065 (2014).
- 7. Zhang, L. L. & Zhao, X. S. Carbon-based materials as supercapacitor electrodes. Chem. Soc. Rev. 38, 2520-2531 (2009).
- 8. Xu, J. et al. A hierarchical carbon derived from sponge-template deactivation of grapheme oxide for high-performance supercapacitor electrodes. Adv. Mater. 28, 5222–5228 (2016).
- 9. Han, X. G. et al. Scalable holey graphene synthesis and dense electrode fabrication toward high-performance ultracapacitors. ACS Nano 8, 8255–8265 (2014).
- A, D. & Hegde, G. Activated carbon nanospheres derived from bio-waste materials for supercapacitor applications-a review. RSC Adv. 5, 88339–88352 (2015).
- 11. Biswal, M., Banerjee, A., Deoab, M. & Ogale, S. From dead leaves to high energy density supercapacitors. *Energy Environ. Sci.* **6**, 1249–1259 (2013).
- 12. Liang, Q. H. et al. A honeycomb-like porous carbon derived from pomelo peel for use in high-performance supercapacitors. Nanoscale 6, 13831–13837 (2014).
- Wang, K. et al. Promising biomass-based activated carbons derived from willow catkins for high performance supercapacitors. Electrochim. Acta 166, 1–11 (2015).
- Xie, L. L. et al. Hierarchical porous carbon microtubes derived from willow catkins for supercapacitor applications. J. Mater. Chem. A. 4, 1637–1646 (2016).
- A. 4, 1037–1046 (2016).
 Li, Z. et al. Carbonized chicken eggshell membranes with 3D architectures as high-performance electrode materials for supercapacitors. Adv. Energy Mater. 2, 431–437 (2012).
- Raymundo-Piñero, E., Cadekand, M. & Béguin, F. Tuning carbon materials for supercapacitors by direct pyrolysis of seaweeds. Adv. Funct. Mater. 19, 1032–1039 (2009).
- Chen, C. et al. Three-dimensional scaffolding framework of porous carbon nanosheets derived from plant wastes for high-performance supercapacitors. Nano Energy 27, 377–389 (2016).
- Hou, J. H., Cao, C. B., Idrees, F. & Ma, X. L. Hierarchical porous nitrogen-doped carbon nanosheets derived from silk for ultrahigh-capacity battery anodes and supercapacitors. ACS Nano 9, 2556–2564 (2015).
- 19. Yun, Y. S. *et al.* Microporous carbon nanoplates from regenerated silk proteins for supercapacitors. *Adv. Mater.* **25**, 1993–1998 (2013)
- 20. Rufford, T. E. et al. Microstructure and electrochemical double-layer capacitance of carbon electrodes prepared by zinc chloride activation of sugar cane bagasse. *J. Power Sources* 195, 912–918 (2010).
- 21. Yun, Y. S. et al. Hierarchically porous carbon nanosheets from waste coffee grounds for supercapacitors. ACS Appl. Mater. Interfaces 7, 3684–3690 (2015).
- Dolah, B. N. M. et al. A method to produce binderless supercapacitor electrode monoliths from biomass carbon and carbon nanotubes. Materials Research Bulletin 60, 10–19 (2014).
- 23. Wang, X. J. et al. All-biomaterial supercapacitor derived from bacterial cellulose. Nanoscale 8, 9146-9150 (2016).
- Wu, X. L. et al. Biomass-derived sponge-like carbonaceous hydrogels and aerogels for supercapacitors. ACS Nano 7, 3589–3597 (2013).
- 25. Li, L. et al. Nitrogen-doped carbonized cotton for highly flexible supercapacitors. Carbon 105, 260-267 (2016).
- 26. Li, H. B. et al. Carbonized-leaf membrane with anisotropic surfaces for sodium-ion battery. ACS Appl. Mater. Interfaces 8, 2204–2210 (2016)
- 27. Chen, T. & Dai, L. M. Flexible supercapacitors based on carbon nanomaterials. *J. Mater. Chem.A* 2, 10756–10775 (2014).
- 28. Li, B. et al. Nitrogen-doped activated carbon for a high energy hybrid supercapacitor. Energy Environ. Sci. 9, 102–106 (2016).
- 29. Schnoor, T. I. W. et al. The production of aligned MWCNT/polypyrrole composite films. Carbon 105, 260-267 (2009).
- 30. Ouyang, A. et al. Polymer-coated graphene aerogel beads and supercapacitor application. Appl. Mater. Interfaces 8, 11179–11187 (2016).
- 31. Zhou Y. et al. Highly flexible all-solid-state supercapacitors based on carbon nanotube/polypyrrole composite films and fibers. RSC Adv. 6, 62062–62070 (2016).
- 32. Sun, H. et al. Large-area supercapacitor textiles with novel hierarchical conducting structures. Adv. Mater. 28, 8431-8438 (2016).
- 33. Sun, H. et al. A novel slicing method for thin supercapacitors. Adv. Mater. 28, 6429-6435 (2016).
- 34. He, S. S. et al. A three-dimensionally stretchable high performance supercapacitor. J. Mater. Chem. A 4, 14968-14973 (2016).
- 35. Senthilkumar, S. T. et al. Flexible fiber hybrid supercapacitor with NiCo₂O₄ nanograss@carbon fiber and bio-waste derived high surface area porous carbon. Electrochim. Acta 211, 411–419 (2016).
- 36. Hasegawa, G. et al. Hierarchically porous carbon monoliths comprising ordered mesoporous nanorod assemblies for high-voltage aqueous supercapacitors. Chem. Mater. 28, 3944–3950 (2016).
- 37. Jiang, L. L. et al. Construction of nitrogen-doped porous carbon buildings using interconnected ultra-small carbon nanosheets for ultra-high rate supercapacitors. J. Mater. Chem. A 4, 11388–11396 (2016).

Acknowledgements

We thank Mr. Feng Yuan in Beijing Urban Construction Design & Development Group Co., Limited (UCD) for drawing the petals in the schematic illustration in Figure 1a. This work was supported by Outstanding Young Talent Research Fund of Zhengzhou University (1521317003); National Natural Science Foundation under grants of NSFC 51502267 and Certificate of Postdoctoral Research Sponsorship Henan Province (2015009).

Author Contributions

H.B.L. and Y.Y.S. devised the original concept, designed the experiment, discussed the results and co-wrote the paper. X.X.Y., Y.W. and L.L. performed the experiments and analyzed the data. All authors reviewed the manuscript.

Additional Information

Supplementary information accompanies this paper at http://www.nature.com/srep

Competing Interests: The authors declare no competing financial interests.

How to cite this article: Yu, X. et al. Soft and wrinkled carbon membranes derived from petals for flexible supercapacitors. Sci. Rep. 7, 45378; doi: 10.1038/srep45378 (2017).

Publisher's note: Springer Nature remains neutral with regard to jurisdictional claims in published maps and institutional affiliations.

This work is licensed under a Creative Commons Attribution 4.0 International License. The images or other third party material in this article are included in the article's Creative Commons license, unless indicated otherwise in the credit line; if the material is not included under the Creative Commons license, users will need to obtain permission from the license holder to reproduce the material. To view a copy of this license, visit http://creativecommons.org/licenses/by/4.0/

© The Author(s) 2017



OPEN Corrigendum: Soft and wrinkled carbon membranes derived from petals for flexible supercapacitors

Xiuxiu Yu, Ying Wang, Li Li, Hongbian Li & Yuanyuan Shang

Scientific Reports 7:45378; doi: 10.1038/srep45378; published online 31 March 2017; updated 08 January 2018

In the original version of this Article, Li Li and Hongbian Li were incorrectly affiliated with 'CAS Center for Excellence in Nanoscience, 11, Beiyitiao, Zhonguancun, Beijing, 100190, China. The correct affiliations for Li Li and Hongbian Li are listed below.

CAS Center for Excellence in Nanoscience, National Center for Nanoscience and Technology, Beijing, 100190, China

University of Chinese Academy of Sciences, Beijing, 100049, China.

This error has now been corrected in the PDF and HTML versions of the Article.

This work is licensed under a Creative Commons Attribution 4.0 International License. The images or other third party material in this article are included in the article's Creative Commons license, unless indicated otherwise in the credit line; if the material is not included under the Creative Commons license, users will need to obtain permission from the license holder to reproduce the material. To view a copy of this license, visit http://creativecommons.org/licenses/by/4.0/

© The Author(s) 2018